Smoothly Switched Adaptive Torque Tracking for Functional Electrical Stimulation Cycling

Jace B. Aldrich and Christian A. Cousin

***Abstract*—Motorized functional electrical stimulation (FES) cycling can serve as a rehabilitation strategy for individuals affected by neurological injuries. It is unique among human-robot interaction tasks because the cycle's motor must be simultaneously controlled alongside the rider's leg muscles (using neuromuscular electrical stimulation). In this letter, two tracking objectives are proposed for the FES cycle: 1) stimulate the rider's leg muscles to track a desired cadence, and 2) use the cycle's motor to indirectly track a desired torque with an adaptive admittance controller. A combined Lyapunov and passivity based switched systems stability analysis is conducted to prove the cycle's motor is able to globally exponentially track the admittance trajectory and stabilize the overall system. Additionally, this letter showcases a method for the rider to smoothly enable and disable torque tracking. Experiments are presented on four participants to show the efficacy of the controllers.**

***Index Terms*—Lyapunov, nonlinear, admittance, passivity, rehabilitation.**

I. Introduction

WORLDWIDE, millions of people are affected by neurological injuries such as stroke and spinal cord injuries [1], [2]. Because these injuries can result in movement impairments (e.g., general paresis or paralysis), they can severely compromise an individual's ability to control their neuromuscular system and negatively affect an individual's quality of life and activities of daily living. Moreover, these injuries can result in highly sedentary lifestyles and lead to a host of negative secondary health effects [3]. While there are numerous options for rehabilitation, motorized functional electrical stimulation (FES) cycles combine two common options: FES and rehabilitation robotics [4].

While FES has been shown to impart a number of benefits for those with mobility impairments [5], [6], it is difficult to accurately control due to dynamic nonlinearities and time-varying characteristics of muscle contractions [7]. Similarly, rehabilitation robotics offer a number of benefits [8], but because they involve intimate human-robot interaction, they must be well controlled to preserve human safety. When rehabilitation robots are physically coupled to a human, they can be considered exoskeletons; when FES is combined with an exoskeleton, it can be considered a hybrid exoskeleton [9], [10].

FES cycles are examples of hybrid exoskeletons and utilize both FES to stimulate the rider's leg muscles and an electric motor to actuate the combined system. FES cycles can be controlled a number of ways, but among the most common methods are cadence control [4], [11] or cadence/torque control [12]. To prove stability and guarantee safety, controllers should be accompanied with a switched systems stability analysis [4].

Torque control of FES cycling can be done directly [13] or indirectly using an admittance filter and controller [12]. Admittance control is widely used for human-robot interaction [14], [15], rehabilitation tasks [16], [17], and is viewed as an assist-as-needed control paradigm, where a robot can assist a human to various degrees [14], [16]. Moreover, admittance control is amenable to adaptation both in the inner-loop position controller, and in the outer-loop of force control [18], [19]. While admittance control (and by extension, torque control) has been used on FES cycles previously, to the best of the authors' knowledge, the torque/admittance error systems are active at all times (e.g., [12], [19]), or only in regions where it is kinematically efficient (e.g., [20]). Consequently, the rider's muscles can quickly fatigue, become saturated with stimulation, contribute diminishing amounts of torque (see [13]), and result in diminished benefits. Therefore, it may be desirable to periodically withdraw stimulation over the course of a rehabilitation session.

In this letter, two tracking objectives are proposed for the FES cycle: 1) stimulate the rider's leg muscles to track a desired cadence, and 2) use the cycle's motor to indirectly track a desired torque using an adaptive admittance controller. Compared to our past results, the admittance filter now adapts to support yet continuously challenge the rider in their cadence tracking task. Additionally, the rider is now able to manually enable/disable torque tracking and use the cycle's motor to smoothly take over the cadence tracking objective. This strategy allows the rider to reduce stimulation, avoid excessive fatigue, and recover before re-enabling torque tracking.

Moreover, the stimulation controller is continuous—which eliminates all high-frequency feedback—and saturated in the

Manuscript received March 16, 2021; revised May 13, 2021; accepted May 30, 2021. Date of publication June 7, 2021; date of current version June 30, 2021. Recommended by Senior Editor F. Dabbene. *(Corresponding author: Christian A. Cousin.)*

The authors are with the Department of Mechanical Engineering, University of Alabama, Tuscaloosa, AL 35401 USA (e-mail: jbaldrich@crimson.ua.edu; cacousin@eng.ua.edu).

Digital Object Identifier 10.1109/LCSYS.2021.3086772

stability analysis, opposed to solely in implementation (exception in [19]). The admittance tracking objective is prioritized over the cadence tracking objective and using a Lyapunov based switched systems stability analysis, it is shown that the cycle's motor is able to globally exponentially track the admittance trajectory. A passivity based switched systems stability analysis is conducted to show the cadence error system is output-feedback passive and that the adaptive admittance filter is output-strictly passive. When torque tracking is disabled, the admittance trajectory smoothly aligns with the cadence trajectory, and the motor is able to guarantee global exponentially tracking of the desired cadence. Experiments are presented on four able-bodied participants to show the efficacy of the controllers.

II. Dynamics

A. Human Rider Model

The human subsystem dynamics are based on [4] as[1]

$$M_h(q)\ddot{q} + C_h(q,\dot{q})\dot{q} + G_h(q) + P(q,\dot{q}) + d_h(t) = \tau_{int}(t) + \tau_h(q,\dot{q},t), \tag{1}$$

where $q : \mathbb{R}_{\geq t_0} \to \mathcal{Q}$ denotes the measurable crank angle of the cycle, the set $\mathcal{Q} \subseteq \mathbb{R}$ contains all possible crank angles, $t_0 \in \mathbb{R}_{\geq 0}$ denotes the initial time, $\dot{q} : \mathbb{R}_{\geq t_0} \to \mathbb{R}$ denotes the measurable angular velocity of the crank (i.e., cadence), and $\ddot{q} : \mathbb{R}_{\geq t_0} \to \mathbb{R}$ denotes the unknown angular acceleration. The inertial, centripetal-Coriolis, and gravitational effects of the rider are denoted by $M_h : \mathcal{Q} \to \mathbb{R}$, $C_h : \mathcal{Q} \times \mathbb{R} \to \mathbb{R}$, and $G_h : \mathcal{Q} \to \mathbb{R}$, respectively. The rider's passive viscoelastic tissue torques and disturbances (e.g., reflexes and voluntary contributions) are denoted by $P : \mathcal{Q} \times \mathbb{R} \to \mathbb{R}$ and $d_h : \mathbb{R}_{\geq t_0} \to \mathbb{R}$, respectively, and the measurable bounded interaction torque between the rider and cycle is denoted by $\tau_{int} : \mathbb{R}_{\geq t_0} \to \mathbb{R}$ [21]. The torque from the rider's muscles is denoted by $\tau_h : \mathcal{Q} \times \mathbb{R} \times \mathbb{R}_{\geq t_0} \to \mathbb{R}$ and defined as

$$\tau_h(q,\dot{q},t) \triangleq B_h(q,\dot{q})u_h(t), \tag{2}$$

where $u_h : \mathbb{R}_{\geq t_0} \to \mathbb{R}$ denotes the subsequently designed muscle control input and $B_h : \mathcal{Q} \times \mathbb{R} \to \mathbb{R}_{>0}$ denotes a lumped muscle control effectiveness defined as

$$B_h(q,\dot{q}) \triangleq \sum_{m\in\mathcal{M}} b_m(q,\dot{q})k_m\sigma_m(q,\dot{q}), \tag{3}$$

where $b_m : \mathcal{Q} \times \mathbb{R} \to \mathbb{R}_{>0}$ denotes the unknown, nonlinear individual muscle control effectiveness mapping the FES input to muscle output torque, $k_m \in \mathbb{R}_{>0}$ denotes an individual muscle group's control gain, and $\sigma_m : \mathcal{Q} \times \mathbb{R} \to \{0,1\}$ denotes the subsequently designed piecewise right-continuous switching signal for activating individual muscle groups. The set $\mathcal{M}$ includes the rider's right and left quadriceps femoris, hamstring, and gluteal muscle groups.

[1]For notational brevity, all explicit dependence on time, t, within the states $q(t), \dot{q}(t), \ddot{q}(t)$ is suppressed.

B. Motorized Cycle Model

The robot subsystem dynamics, which consist of a motorized recumbent tricycle, are based on [4] as

$$M_r(q)\ddot{q} + C_r(q,\dot{q})\dot{q} + G_r(q) + b\dot{q} + d_r(t) = -\tau_{int}(t) + \tau_r(t), \tag{4}$$

where $M_r : \mathcal{Q} \to \mathbb{R}$, $C_r : \mathcal{Q} \times \mathbb{R} \to \mathbb{R}$, and $G_r : \mathcal{Q} \to \mathbb{R}$ denote the cycle's inertial, centripetal-Coriolis, and gravitational effects, respectively. The torques resulting from viscous friction and unknown disturbances are denoted by $b : \mathbb{R}_{>0} \to \mathbb{R}$ and $d_r : \mathbb{R}_{\geq t_0} \to \mathbb{R}$, respectively. The torque applied about the crank axis by the cycle's electric motor is denoted by $\tau_r : \mathbb{R}_{\geq t_0} \to \mathbb{R}$, which can be expressed as

$$\tau_r(t) \triangleq B_r u_r(t), \tag{5}$$

where $B_r \in \mathbb{R}_{>0}$ denotes the known motor constant relating the motor's input current to output torque, and $u_r : \mathbb{R}_{\geq t_0} \to \mathbb{R}$ denotes the subsequently designed motor control input.

C. Switching Model

The switching signal σ_m in (3) is used to activate and deactivate each muscle group, and is defined as $\sigma_m(q,\dot{q}) \triangleq 1$ if $q^* \in \mathcal{Q}_m$, and $\sigma_m(q,\dot{q}) \triangleq 0$ if $q^* \notin \mathcal{Q}_m$, $\forall m \in \mathcal{M}$ where $q^* : \mathcal{Q} \times \mathbb{R} \to \mathcal{Q}$ denotes an advanced crank angle defined as $q^* \triangleq q + 0.1\dot{q}$, incorporated to account for the electromechanical delay in stimulated muscles [22]. Above, $\mathcal{Q}_m \subset \mathcal{Q}$ denotes the regions in which muscle group m is able to supply a positive torque about the crank [4]. The union of all muscle stimulation regions establishes the FES region of the crank cycle, defined as $\mathcal{Q}_M \triangleq \bigcup_{m\in\mathcal{M}} \mathcal{Q}_m$, and the kinematic deadzone (KDZ) as the remainder $\mathcal{Q}_K \triangleq \mathcal{Q} \backslash \mathcal{Q}_M$.

Because the switching signal σ_m is used to discretely activate the rider's muscle groups, it is discontinuous by design. Hence, the torque input to the system discretely changes, but the states continuously evolve. The combination of discretely changing control inputs with continuous state dynamics gives rise to a state-dependent switched system. To facilitate the following analysis, the following properties are provided for the systems in (1) and (4).

Property 1: The dynamic functions M_x, C_x, G_x, d_x, P, b have known bounds given by $c_{m_x} \leq M_x(q) \leq c_{M_x}$, $|C_x(q,\dot{q})| \leq c_{C_x}|\dot{q}|$, $|G_x(q)| \leq c_{G_x}$, $|d_x(t)| \leq c_{d_x}$, $|P(q,\dot{q})| \leq c_{P1} + c_{P2}|\dot{q}|$, and $b \leq c_b$, respectively, where c_{m_x}, c_{M_x}, c_{C_x}, c_{G_x}, c_{P1}, c_{P2}, c_b, $c_{d_x} \in \mathbb{R}_{>0}$ are known constants $\forall x \in \{h, r\}$ [4].

Property 2: The inertia and centripetal-Coriolis terms are skew-symmetric, $\dot{M}(q) - 2C(q,\dot{q}) = 0$ [23].

Property 3: Although the muscle control effectiveness b_m is subject to nonlinear activation dynamics and a muscle fiber recruitment curve [24]–[27], it can be generalized as a function of $q(t)$ and $\dot{q}(t)$ [4]. Furthermore, when $q^* \in \mathcal{Q}_M$, B_h is bounded by $B_{\underline{h}} \leq B_h(q,\dot{q}) \leq B_{\overline{h}}$, where $B_{\underline{h}}$, $B_{\overline{h}} \in \mathbb{R}_{>0}$ are known constants [26].

III. Control Development

To actuate the combined system, two independent but coupled tracking objectives and controllers are developed. The

admittance filter is adaptive and assists yet continuously challenges the rider, and the rider can manually enable and disable torque tracking with an external switch on the cycle. Because two tracking objectives are presented for two subsystems, two controllers are required for implementation.

A. Error System Development

The cadence tracking objective is quantified by the position tracking error $e : \mathbb{R}_{\geq t_0} \to \mathbb{R}$ and the filtered tracking error $r : \mathbb{R}_{\geq t_0} \to \mathbb{R}$, defined as[2]

$$e(t) \triangleq q_d - q, \tag{6}$$

$$r(t) \triangleq \dot{e} + \alpha e, \tag{7}$$

respectively, where $q_d : \mathbb{R}_{\geq t_0} \to \mathbb{R}$ denotes the twice differentiable ($q_d \in \mathcal{C}^2$) desired position trajectory, and $\alpha \in \mathbb{R}_{>0}$ denotes a selectable control gain. To facilitate the following analysis, let $z : \mathbb{R}_{\geq t_0} \to \mathbb{R}^2$ denote a composite error vector defined as $z(t) \triangleq [e \quad r]^T$. The indirect torque tracking objective is quantified by the admittance position tracking error $\xi : \mathbb{R}_{\geq t_0} \to \mathbb{R}$ and the filtered admittance tracking error $\psi : \mathbb{R}_{\geq t_0} \to \mathbb{R}$, defined as

$$\xi(t) \triangleq q_a + q_d - q, \tag{8}$$

$$\psi(t) \triangleq \dot{\xi} + \beta \xi, \tag{9}$$

respectively, where $q_a : \mathbb{R}_{\geq t_0} \to \mathcal{Q}$ denotes the generated admittance position trajectory, and $\beta \in \mathbb{R}_{>0}$ denotes a selectable control gain. Let $\zeta : \mathbb{R}_{\geq t_0} \to \mathbb{R}^2$ denote a composite error vector defined as $\zeta(t) \triangleq [\xi \quad \psi]^T$. The admittance cadence trajectory $\dot{q}_a$ is generated online through an adaptive admittance filter designed as

$$e_\tau(t) \triangleq M_d \ddot{q}_a + \hat{B}_d(t) \dot{q}_a, \tag{10}$$

where $M_d \in \mathbb{R}_{>0}$ denotes a constant filter parameter and $\hat{B}_d : \mathbb{R}_{\geq t_0} \to \mathbb{R}_{\geq 0}$ denotes an adaptive damping parameter. To continuously support and challenge the rider, the damping parameter is propagated online according to the update law

$$\dot{\hat{B}}_d \triangleq \Gamma_l \dot{q}_a^2 - \Gamma_f \hat{B}_d, \tag{11}$$

where $\Gamma_l \in \mathbb{R}_{>0}$ denotes a selectable learning gain and $\Gamma_f \in \mathbb{R}_{>0}$ denotes a selectable forgetting factor. In (10), the interaction torque error between the rider and the cycle is denoted by $e_\tau : \mathbb{R}_{\geq 0} \to \mathbb{R}$ and defined as

$$e_\tau(t) \triangleq \tau_d^*(t) - \tau_{int}^*(t), \tag{12}$$

where $\tau_d^* : \mathbb{R}_{\geq 0} \to \mathbb{R}$ denotes a continuously differentiable ($\tau_d^* \in \mathcal{C}^1$), time-varying, scaled desired interaction torque and $\tau_{int}^* : \mathbb{R}_{\geq 0} \to \mathbb{R}$ denotes a continuous ($\tau_{int}^* \in \mathcal{C}^0$) scaled interaction torque defined as

$$\tau_{int}^*(t) \triangleq \tau_d^{-1} \tau_d^*(t) \tau_{int}(t). \tag{13}$$

In (13), $\tau_d \in \mathbb{R}$ denotes a selectable, bounded constant desired interaction torque ($\tau_d \in \mathcal{L}_\infty$).

[2]For notational brevity, all functional dependencies are hereafter suppressed unless required for clarity of exposition.

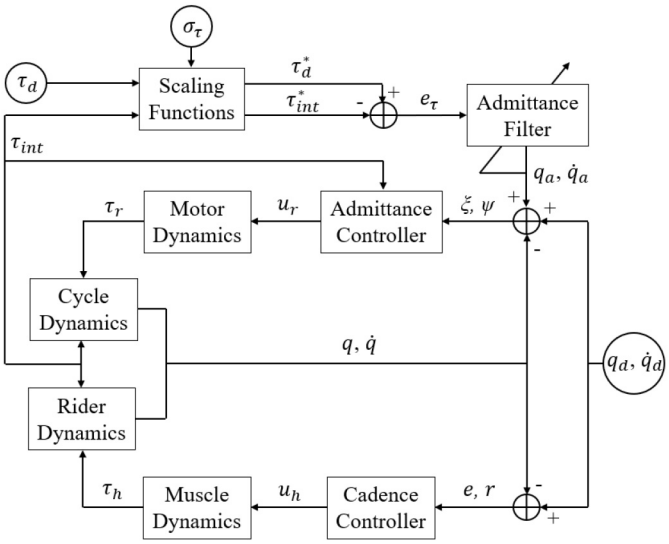

Fig. 1. Block diagram depicting the closed-loop cadence and admittance controllers, the adaptive admittance filter, and the torque scaling functions in (13) and (14). Circles denote inputs to the combined cycle-rider system.

The time-varying desired torque in (12) and (13) is generated online according to the polynomial

$$\tau_d^*(t) \triangleq \begin{cases} a_1 + a_2\left(t - t_0^n\right)^2 + a_3\left(t - t_0^n\right)^3 & t - t_0^n \leq \Delta t \\ \sigma_\tau \tau_d & t - t_0^n > \Delta t, \end{cases} \tag{14}$$

where $\sigma_\tau : \mathbb{R}_{\geq t_0} \to \{0, 1\}$ denotes a piecewise right-continuous torque tracking switching signal and where the coefficients are defined as $a_1 \triangleq (1 - \sigma_\tau)\tau_d$, $a_2 \triangleq \frac{3}{\Delta t^2}(2\sigma_\tau - 1)\tau_d$, and $a_3 \triangleq \frac{-2}{\Delta t^3}(2\sigma_\tau - 1)\tau_d$. In (14), the term $t_0^n \in \mathbb{R}_{\geq t_0}$ denotes the time of the nth triggering of σ_τ, and $\Delta t \in \mathbb{R}_{>0}$ denotes a selectable scaling window. To enable and disable torque tracking, the rider sets $\sigma_\tau = 1$ and $\sigma_\tau = 0$, respectively. The control structure is depicted in Figure 1.

B. Admittance Controller

To develop the admittance controller used by the cycle's motor, the open-loop admittance error system is generated by taking the time derivative of (9), multiplying by M_r, adding and subtracting ξ, and substituting (4) and (6)-(9) to yield

$$M_r \dot{\psi} = \chi_1 - \tau_r + \tau_{int} - C_r \psi - \xi. \tag{15}$$

The lumped auxiliary signal $\chi_1 : \mathbb{R}^4 \times \mathbb{R}_{\geq 0} \to \mathbb{R}$ denotes system disturbances and is bounded by Property 1 as $|\chi_1| \leq c_1 + c_2\|\phi\| + c_3\|\phi\|^2$, where $c_1, \ c_2, \ c_3 \in \mathbb{R}_{>0}$ are known constants, and $\phi \triangleq [\xi \quad \psi \quad \dot{q}_a \quad \ddot{q}_a]^T$. Based on (15) and the subsequent stability analysis, the admittance controller is designed as

$$u_r \triangleq \frac{1}{B_r}\left(k_1 \psi + \tau_{int} + \left(k_2 + k_3\|\phi\| + k_4\|\phi\|^2\right)\text{sgn}(\psi)\right) \tag{16}$$

where $k_i \in \mathbb{R}_{>0} \ \forall i = \{1, 2, 3, 4\}$ denote constant control gains, and B_r is introduced in (5). Substituting (5) and (16) into (15) yields the closed-loop admittance error system

$$M_r \dot{\psi} = \chi_1 - k_1 \psi - \left(k_2 + k_3\|\phi\| + k_4\|\phi\|^2\right)\text{sgn}(\psi) - C_r \psi - \xi. \tag{17}$$

C. Cadence Controller

To develop the cadence controller used to stimulate the rider's muscles, the open-loop cadence error system is generated by taking the time derivative of (7), multiplying by M_h, adding and subtracting e, and substituting (1), (6), and (7) to yield

$$M_h\dot{r} = \chi_2 - \tau_h - \tau_{int} - C_h r - e. \tag{18}$$

The lumped auxiliary signal $\chi_2 : \mathbb{R}^2 \times \mathbb{R}_{\geq 0} \to \mathbb{R}$ denotes system disturbances and is bounded by Property 1 as $|\chi_2| \leq c_4 + c_5\|z\| + c_6\|z\|^2$, where $c_4,\ c_5,\ c_6 \in \mathbb{R}_{>0}$ are known constants. Based on (18) and the subsequent stability analysis, the cadence controller is designed as

$$u_h \triangleq \text{sat}_\mu\left[B_{\underline{h}}^{-1} k_5 r\right], \tag{19}$$

where $k_5 \in \mathbb{R}_{>0}$ denotes a constant control gain, $B_{\underline{h}}$ is introduced in Property 3, and $\text{sat}_\mu[x]$ denotes a saturation function defined as $\text{sat}_\mu[x] \triangleq \mu$ if $x > \mu$, $\text{sat}_\mu[x] \triangleq x$ if $0 \leq x \leq \mu$, and $\text{sat}_\mu[x] \triangleq 0$ if $x < 0$. The saturation function is included in the cadence (i.e., muscle) controller to limit the amount of stimulation delivered to the rider for comfort and safety, and the saturation limit $\mu \in \mathbb{R}_{>0}$ is selected by the rider during IRB-approved pretests. Substituting (2), (3), and (19) into (18) yields the closed-loop cadence error system

$$M_h\dot{r} = \chi_2 - B_h \text{sat}_\mu\left[B_{\underline{h}}^{-1} k_5 r\right] - \tau_{int} - C_h r - e. \tag{20}$$

IV. Stability Analysis

When torque tracking is enabled, the admittance and cadence error systems are independent; however, when torque tracking is disabled, the admittance error system smoothly merges with the cadence error system. For this reason, the admittance error system is selected as the dominant, or convergent, error system. Theorem 1 uses a Lyapunov-like switched system stability analysis to guarantee the closed-loop admittance error system in (17) is exponentially driven to zero. Theorem 2 uses a passivity analysis for switched systems to conclude the closed-loop cadence error system in (20) is output-feedback passive. Theorem 3 uses a passivity analysis to prove the admittance filter is output-strictly passive. To facilitate the following analysis, let $V_1 : \mathbb{R}^2 \to \mathbb{R}$ denote a positive-definite candidate Lyapunov function defined as

$$V_1(\zeta) \triangleq \frac{1}{2} M_r \psi^2 + \frac{1}{2}\xi^2, \tag{21}$$

where $V_1(\zeta)$ can be bounded by Property 1 as $\lambda_1\|\zeta\|^2 \leq V_1(\zeta) \leq \lambda_2\|\zeta\|^2$, and $\lambda_1,\ \lambda_2 \in \mathbb{R}_{>0}$ are known constants defined as $\lambda_1 \triangleq \frac{1}{2}\min(c_m, 1)$ and $\lambda_2 \triangleq \frac{1}{2}\max(c_M, 1)$. Furthermore, let $V_2 : \mathbb{R}^2 \to \mathbb{R}$ and $V_3 : \mathbb{R}^2 \to \mathbb{R}$ denote positive-definite storage functions defined as

$$V_2(z) \triangleq \frac{1}{2} M_h r^2 + \frac{1}{2} e^2, \tag{22}$$

$$V_3\left(\dot{q}_a, \hat{B}_d\right) \triangleq \frac{1}{2}\dot{q}_a^2 + \frac{1}{2}\hat{B}_d^2. \tag{23}$$

Theorem 1: Given the closed-loop admittance error system in (17), the admittance error system is globally exponentially stable in the sense that

$$\|\zeta(t)\| \leq \sqrt{\frac{\lambda_2}{\lambda_1}}\|\zeta(t_0)\| \exp\left[-\frac{\min(k_1, \beta)}{2\lambda_2}(t - t_0)\right], \tag{24}$$

$\forall t \in [t_0, \infty)$, provided the gains in (16) are selected according to the sufficient conditions: $k_2 \geq c_1$, $k_3 \geq c_2$, $k_4 \geq c_4$.

Proof: Using an approach similar to [13], it can be shown that because of the discontinuity in the motor controller in (16), the time derivative of (21) exists almost everywhere (a.e.) (i.e., for almost all $t \in [t_0, \infty)$). After substituting (5), (9), (15), and (16), using Property 2, and canceling cross-terms, the time derivative of (21) can be upper bounded as

$$\dot{V}_1 \overset{\text{a.e.}}{\leq} -\beta\xi^2 - k_1\psi^2 - (k_2 - c_1)|\psi| - (k_3 - c_2)|\psi|\|\phi\| - (k_4 - c_3)|\psi|\|\phi\|^2. \tag{25}$$

Applying the gain conditions listed in Theorem 1, (25) can be further bounded as

$$\dot{V}_1 \overset{\text{a.e.}}{\leq} -\min(k_1, \beta)\|\zeta\|^2. \tag{26}$$

Subsequently, (26) can be used in conjunction with (21) to obtain the result in (24). Since $V_1 > 0$ and $\dot{V}_1 \overset{\text{a.e.}}{\leq} 0$, then $V_1, \xi, \psi \in \mathcal{L}_\infty$. Furthermore, because the admittance filter in (10) is passive,[3] $\dot{q}_a, \ddot{q}_a \in \mathcal{L}_\infty$ and it can be concluded $\|\phi\| \in \mathcal{L}_\infty$. Because $\xi, \psi, \|\phi\| \in \mathcal{L}_\infty$, (16) can be used to show the admittance controller is bounded (i.e., $u_r \in \mathcal{L}_\infty$). Additionally, because the error systems merge when torque tracking is disabled, it can be concluded that the closed-loop cadence error system is globally exponentially bounded when torque tracking is disabled. ■

Theorem 2: The closed-loop cadence error system in (20) is output-feedback passive $\forall t \in [t_0, \infty)$.

Proof: Similar to Theorem 1, because of the discontinuities introduced by the switching signal in (3), the time derivative of (22) exists almost everywhere. After taking the derivative, substituting (2), (7), (18), and (19), using Properties 2 and 3, and canceling cross-terms, the time derivative of (22) can be upper bounded in the FES regions and KDZ as

$$\dot{V}_2 \overset{\text{a.e.}}{\leq} \begin{cases} |\chi_2 + \tau_{int}||r| - B_{\underline{h}}\text{sat}_\mu\left[B_{\underline{h}}^{-1} k_5 r\right] r - \alpha e^2 & q^* \in \mathcal{Q}_\mathcal{M} \\ |\chi_2 + \tau_{int}||r| - \alpha e^2 & q^* \notin \mathcal{Q}_\mathcal{M} \end{cases} \tag{27}$$

respectively. For the case when $q^* \in \mathcal{Q}_\mathcal{M}$, (27) can be further upper bounded for the following saturation cases

$$\dot{V}_2 \overset{\text{a.e.}}{\leq} \begin{cases} |\chi_2 + \tau_{int}||r| - B_{\underline{h}}\mu^2 - \alpha e^2 & B_{\underline{h}}^{-1} k_5 r > \mu \\ |\chi_2 + \tau_{int}||r| - k_5 r^2 - \alpha e^2 & 0 \leq B_{\underline{h}}^{-1} k_5 r \leq \mu \\ |\chi_2 + \tau_{int}||r| - \alpha e^2 & B_{\underline{h}}^{-1} k_5 r < 0. \end{cases} \tag{28}$$

Across all cases (i.e., $\forall q^* \in \mathcal{Q}$), (27) and (28) can be upper bounded as

$$\dot{V}_2 \overset{\text{a.e.}}{\leq} |\tau_{int}|\|z\| + \|z\|\rho_1(\|z\|), \tag{29}$$

where $\rho_1(\|z\|)$ is a known radially unbounded function used to bound χ_2 based on Property 1, i.e., $|\chi_2| \leq \rho_1(\|z\|)$. Hence, (22) is verified as a common storage function across

[3] See Theorem 3.

all regions of the crank cycle, i.e., $\forall q^* \in \mathcal{Q}$. Treating the input to the storage function $V_2(z)$ as $u = |\tau_{int}|$ and the output as $y = \|z\|$, by [28, Definition 6.3], it can then be concluded that the cadence error system is output-feedback passive. Because of the saturation function in (19), the cadence controller is bounded. Hence, it is shown that the cadence error system grows due the interaction torque between the cycle and rider. ■

Remark 1: Because admittance tracking is prioritized over cadence tracking, this shortage of passivity is allowable and does not destabilize the admittance error system.

Theorem 3: Given the adaptive update law in (11), the admittance filter in (10) is output-strictly passive $\forall t \in [t_0, \infty)$, provided the gains in (11) are selected according to the sufficient conditions: $M_d^{-1} \geq \Gamma_l > 0$, $\Gamma_f > 0$.

Proof: Taking the time derivative of (23), substituting (10) and (11), imposing the gain conditions listed in Theorem 3, and upper bounding the result yields

$$\dot{V}_3 \leq M_d^{-1}|e_\tau||\dot{q}_a| - |\dot{q}_a|\rho_2(|\dot{q}_a|), \tag{30}$$

where $\rho_2(|\dot{q}_a|)$ is a radially unbounded function defined as $\rho_2(|\dot{q}_a|) \triangleq (M_d^{-1} - \Gamma_l)\hat{B}_d|\dot{q}_a|$. Treating the input to the storage function $V_3(\dot{q}_a, \hat{B}_d)$ as $u = M_d^{-1}|e_\tau|$ and the output as $y = |\dot{q}_a|$, by [28, Definition 6.3], it can then be concluded that the admittance filter in (10) with the update law (11) is output-strictly passive $\forall t \in [t_0, \infty)$. Hence, the admitted trajectory is bounded and the validity of Theorem 1 is confirmed. ■

V. Experiments

A. Experimental Testbed

The motorized FES cycle was constructed by modifying a recumbent tricycle with an encoder, powermeter, and a 350 W DC motor. The motor was actuated by applying a current according to (16). The rider's feet were securely attached to the cycle's pedals with modified orthotic boots to maintain sagittal alignment of the legs and prevent ankle flexion. The encoder, powermeter, and motor were interfaced with a computer running MATLAB/Simulink/Quarc through a Quanser Q-PIDe data acquisition board sampled at 500 Hz. A Hasomed RehaMove3 stimulator delivered symmetric, biphasic, and rectangular pulses via PALS electrodes. For simplicity, only the rider's quadriceps and hamstrings muscle groups were activated at a frequency of 60 Hz and respective amplitudes of 90 mA and 80 mA. The pulsewidth was modulated automatically by the cadence controller in (19). An emergency stop button was attached to the cycle's handle. Additional details on the testbed are available in [12].

B. Experimental Methods

Experiments were conducted on four able-bodied participants, aged 20-28. The experimental protocol had a total duration of 180 seconds, with the first 30 seconds consisting of a smooth motor-only ramp to the desired cadence of 50 RPM using (16), with $\sigma_\tau = 0$. After the initial ramp, the controllers in (16) and (19) were activated, and the rider was free to enable (and then disable) torque tracking with σ_τ.

TABLE I
Cadence, Tracking, and Power Output Results

Participant	$\dot{q}$ (RPM)	$\dot{q}_a$ (RPM)	$\dot{\xi}$ (RPM)	P (W)
1	48.48±2.62	-1.85±2.56	0.01±0.70	7.27±7.03
2	43.56±12.28	-1.73±2.40	0.23±0.94	2.26±5.47
3	45.69±3.44	-4.31±3.28	0.00±1.24	7.31±13.43
4	45.08±3.68	-4.85±3.56	0.06±2.20	0.44±15.72
Mean	**45.70±6.76**	**-3.18±2.99**	**0.07±1.39**	**4.32±11.26**

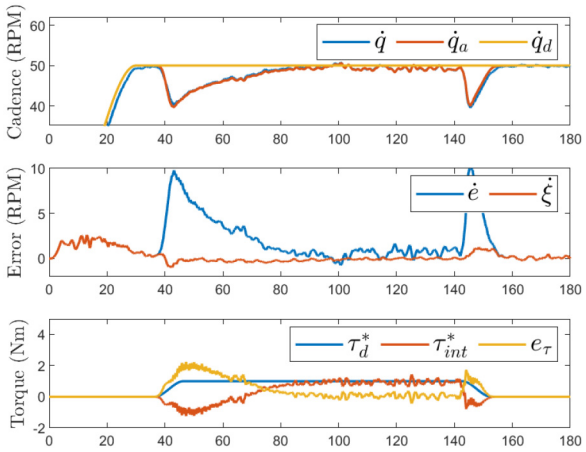

Fig. 2. Tracking results for Participant 1. Torque tracking was enabled at $t \approx 36$ s and disabled at $t \approx 143$ s. For visual clarity, a 1.2 s moving average filter (approximately one crank cycle) was applied to the plots.

For all experiments, the controller gains in (7), (9), (16), and (19) were selected as $k_1 = 3$, $k_2 = k_3 = k_4 = 0.1$, $k_5 = 4$, $\alpha = 1$, $\beta = 0.1$. The update law gains in (11) were selected as $\Gamma_l = 0.5$ and $\Gamma_f = 0.03$. In (10), (13), and (14), the parameters were selected as $M_d = 2\frac{\text{Nm}\cdot\text{s}^2}{\text{rad}}$, $\tau_d \in [0, 1]$ Nm, and $\Delta t = 10$ s. Note, the gain conditions in Theorem 1 are sufficient to achieve stability for the largest uncertainties on the system parameters (established in Properties 1 and 3). These conditions represent the most conservative gains required by the controller in (17) and provide guidelines for the initial gain selection. To achieve desirable performance, gains were subsequently adjusted. All experimental procedures were approved by the University of Alabama, IRB Protocol # 20-005-ME.

C. Results and Discussion

Table I displays the tracking and power output results for all participants. Note, the cycle's cadence ($\dot{q}$), admitted cadence ($\dot{q}_a$), and rider's power output (P) are highly dependent on *when* the rider enabled/disabled torque tracking, and *how long* they enabled tracking. In all experiments, participants enabled and disabled tracking at least once. Regardless of torque tracking, according to Theorem 1, the admittance error should be exponentially driven toward zero with the controller in (16), even in the presence of system disturbances. This effect can be seen by examining the average admittance cadence error, calculated as 0.07 ± 1.39 RPM across all participants.

As shown in Figure 2, when the rider enables torque tracking, the admittance error system smoothly diverges from the cadence error system because of the growth in the interaction

torque error. As the cadence error system increases, so does the rider's stimulation (not pictured). Consequently, the rider's muscles produce an increasing amount of interaction torque, shown in Figure 2. When the rider produces the desired amount of torque, τ_{int}^{*} aligns with τ_{d}^{*}, the admitted cadence tends toward the desired cadence, and both cadence error systems converge toward zero. When the rider disables torque tracking, the torque error smoothly decays to zero due to the scaling functions. Hence, the cycle's motor is capable of smoothly transitioning between the admittance and cadence tracking objectives.

VI. Conclusion

In this letter, the two tracking objectives were presented for a motorized FES cycle. A cadence tracking objective was assigned to the rider's muscles and using a passivity-based analysis, it was shown the closed-loop cadence error system was output-feedback passive. Conversely, the cycle's motor was tasked with indirectly tracking a desired torque using an adaptive admittance filter and controller. Using a Lyapunov-based analysis, it was shown that the closed-loop admittance error system was globally exponentially stable. Using an external trigger, the rider was able to smoothly enable/disable torque tracking and control the behavior of the system. Experiments were performed to show the efficacy of the proposed approach. Future works will include using biological signals (e.g., electromyography) to enable/disable torque tracking and modify trajectories.

References

[1] S. E. Wallace and M. L. Kimbarow, *Cognitive Communication Disorders*. San Diego, CA, USA: Plural, 2016.

[2] E. J. Benjamin *et al.*, "Heart disease and stroke statistics—2017 update," *Circulation*, vol. 135, no. 10, pp. 146–603, 2017.

[3] J. H. Rimmer and J. L. Rowland, "Health promotion for people with disabilities: Implications for empowering the person and promoting disability-friendly environments," *Amer. J. Lifestyle Med.*, vol. 2, no. 5, pp. 409–420, 2008.

[4] M. J. Bellman, R. J. Downey, A. Parikh, and W. E. Dixon, "Automatic control of cycling induced by functional electrical stimulation with electric motor assistance," *IEEE Trans. Autom. Sci. Eng.*, vol. 14, no. 2, pp. 1225–1234, Apr. 2017.

[5] M. Bélanger, R. B. Stein, G. D. Wheeler, T. Gordon, and B. Leduc, "Electrical stimulation: Can it increase muscle strength and reverse osteopenia in spinal cord injured individuals?" *Archives Phys. Med. Rehabil.*, vol. 81, no. 8, pp. 1090–1098, 2000.

[6] S. Ferrante, A. Pedrocchi, G. Ferrigno, and F. Molteni, "Cycling induced by functional electrical stimulation improves the muscular strength and the motor control of individuals with post-acute stroke," *Eur. J. Phys. Rehabil. Med.*, vol. 44, no. 2, pp. 159–167, 2008.

[7] A. J. del Ama, Á. Gil-Agudo, J. L. Pons, and J. C. Moreno, "Hybrid FES-robot cooperative control of ambulatory gait rehabilitation exoskeleton," *J. Neuroeng. Rehabil.*, vol. 11, no. 1, p. 27, 2014.

[8] J. Stein, H. I. Krebs, W. R. Frontera, S. E. Fasoli, R. Hughes, and N. Hogan, "Comparison of two techniques of robot-aided upper limb exercise training after stroke," *Amer. J. Phys. Med. Rehabil.*, vol. 83, no. 9, pp. 720–728, 2004.

[9] A. J. Del-Ama, A. D. Koutsou, J. C. Moreno, A. De-Los-Reyes, Á. Gil-Agudo, and J. L. Pons, "Review of hybrid exoskeletons to restore gait following spinal cord injury," *J. Rehabil. Res. Dev.*, vol. 49, no. 4, pp. 497–514, 2012.

[10] F. Anaya, P. Thangavel, and H. Yu, "Hybrid FES—Robotic gait rehabilitation technologies: A review on mechanical design, actuation, and control strategies," *Int. J. Intell. Robot. Appl.*, vol. 2, pp. 1–28, Jan. 2018.

[11] V. H. Duenas, C. A. Cousin, C. Rouse, E. J. Fox, and W. E. Dixon, "Distributed repetitive learning control for cooperative cadence tracking in functional electrical stimulation cycling," *IEEE Trans. Cybern.*, vol. 50, no. 3, pp. 1084–1095, Mar. 2020.

[12] C. A. Cousin, C. A. Rouse, V. H. Duenas, and W. E. Dixon, "Controlling the cadence and admittance of a functional electrical stimulation cycle," *IEEE Trans. Neural Syst. Rehabil. Eng.*, vol. 27, no. 6, pp. 1181–1192, Jun. 2019.

[13] C. A. Cousin *et al.*, "Closed-loop cadence and instantaneous power control on a motorized functional electrical stimulation cycle," *IEEE Trans. Control Syst. Technol.*, vol. 28, no. 6, pp. 2276–2291, Nov. 2020.

[14] I. Ranatunga, F. L. Lewis, D. O. Popa, and S. M. Tousif, "Adaptive admittance control for human–robot interaction using model reference design and adaptive inverse filtering," *IEEE Trans. Control Syst. Technol.*, vol. 25, no. 1, pp. 278–285, Jan. 2017.

[15] Z. Li, B. Huang, Z. Ye, M. Deng, and C. Yang, "Physical human–robot interaction of a robotic exoskeleton by admittance control," *IEEE Trans. Ind. Electron.*, vol. 65, no. 12, pp. 9614–9624, Dec. 2018.

[16] Q. Wu, X. Wang, B. Chen, and H. Wu, "Development of a minimal-intervention-based admittance control strategy for upper extremity rehabilitation exoskeleton," *IEEE Trans. Syst., Man, Cybern., Syst.*, vol. 48, no. 6, pp. 1005–1016, Jun. 2018.

[17] M. S. Ayas and I. H. Altas, "Fuzzy logic based adaptive admittance control of a redundantly actuated ankle rehabilitation robot," *Control Eng. Pract.*, vol. 59, pp. 44–54, Feb. 2017.

[18] C. A. Cousin, P. Deptula, C. Rouse, and W. E. Dixon, "Cycling with functional electrical stimulation and adaptive neural network admittance control," in *Proc. Amer. Control Conf.*, 2019, pp. 1742–1747.

[19] C. A. Cousin, C. A. Rouse, and W. E. Dixon, "Split-crank functional electrical stimulation cycling: An adapting admitting rehabilitation robot," *IEEE Trans. Control Syst. Technol.*, early access, Nov. 4, 2020, doi: 10.1109/TCST.2020.3032474.

[20] V. Duenas, C. A. Cousin, V. Ghanbari, E. J. Fox, and W. E. Dixon, "Torque and cadence tracking in functional electrical stimulation induced cycling using passivity-based spatial repetitive learning control," *Automatica*, vol. 115, pp. 1–9, May 2020.

[21] Y. Li and S. S. Ge, "Impedance learning for robots interacting with unknown environments," *IEEE Trans. Control Syst. Technol.*, vol. 22, no. 4, pp. 1422–1432, Jul. 2014.

[22] R. Downey, M. Merad, E. Gonzalez, and W. E. Dixon, "The time-varying nature of electromechanical delay and muscle control effectiveness in response to stimulation-induced fatigue," *IEEE Trans. Neural Syst. Rehabil. Eng.*, vol. 25, no. 9, pp. 1397–1408, Sep. 2017.

[23] A. Behal, W. E. Dixon, B. Xian, and D. M. Dawson, *Lyapunov-Based Control of Robotic Systems*. Singapore: Taylor and Francis, 2009.

[24] D. B. Popović, "Advances in functional electrical stimulation," *J. Electromyography Kinesiol.*, vol. 24, no. 6, pp. 795–802, Dec. 2014.

[25] M. Ferrarin, F. Palazzo, R. Riener, and J. Quintern, "Model-based control of FES-induced single joint movements," *IEEE Trans. Neural Syst. Rehabil. Eng.*, vol. 9, no. 3, pp. 245–257, Sep. 2001.

[26] N. Sharma, K. Stegath, C. M. Gregory, and W. E. Dixon, "Nonlinear neuromuscular electrical stimulation tracking control of a human limb," *IEEE Trans. Neural Syst. Rehabil. Eng.*, vol. 17, no. 6, pp. 576–584, Dec. 2009.

[27] N. Sharma, N. A. Kirsch, N. A. Alibeji, and W. E. Dixon, "A nonlinear control method to compensate for muscle fatigue during neuromuscular electrical stimulation," *Front. Robot. AI*, vol. 4, p. 68, Dec. 2017.

[28] H. K. Khalil, *Nonlinear Systems*, 3rd ed. Upper Saddle River, NJ, USA: Prentice-Hall, 2002.